PCCP

Accepted Manuscript

ROYAL SOCIETY OF CHEMISTRY

www.rsc.org/pccp

Journal Name

RSCPublishing

ARTICLE

Cyano-Substituted Oligo(p-phenylene vinylene) Single-crystal with balanced hole and electron injection and transport for Ambipolar Field-effect Transistor

Cite this: DOI: 10.1039/x0xx00000x

Received 00th January 2012,
Accepted 00th January 2012

DOI: 10.1039/x0xx00000x

www.rsc.org/

Jian Deng,[a] Jia Tang,[a] Yuanxiang Xu,[a] Liqun Liu,[a] Yan Wang,[*,b] Zengqi Xie,[c] and Yuguang Ma[*,a]

High and balanced hole and electron mobilities were achieved in OFET based on the high photoluminescence 1,4-bis(2-cyano-2-phenylethenyl)benzene single-crystal with symmetric gold electrodes. For electron and hole, the operation voltage was 30 and -20 V, the accumulation threshold voltage is low enough for the OFETs to operate in ambipolar model with the source/drain voltage (V_{ds}) around 50 V despite the high injection barrier. The highest electron and hole mobility was 0.745 $cm^2V^{-1}s^{-1}$ and 0.239 $cm^2V^{-1}s^{-1}$, and the current density reached 90.7 and 27.4 A/cm^2 with assumed 10 nm accumulation layer. The high mobility comes from the strong π-π interaction, in addition, the highly order hydrogen bonding matrix may create an efficient route to pump the charge to the inner layer which can improve the injection ability.

Introduction

Organic single crystals constructed by π-π stacking have been widely studied during the past years.[1-5] Owing to the well-defined structure, the organic crystals provide extremely clear models to investigate the relationship between supramolecular interaction and the stacking model, and their influence on the optical and electric properties.[6, 7] The highly ordered π-π stacking leads the organic single-crystals trend to higher mobility than amorphous thin films, which makes them incredibly attractive in fabricating high performance optoelectronic devices such as optically pumped lasers,[8, 9] field-effect transistors (FETs)[10] and photovoltaic cells[11].

So far, though some single-crystals have demonstrated balanced mobility,[12, 13] most single-crystal ambipolar organic FETs (OFETs) have still demonstrated electron mobility at least one order of magnitude lower than the hole's.[14-18] However, to ensure more efficient recombination and higher current density, improving the electron injection and transport become a very emergent issue. Trans-1,4-distyrylbenzene (trans-DSB) is a simple model compound developed to investigate the internal relationship of optoelectronic characters, chemical structure, and interactions between molecules in the solid of poly(p-phenylene vinylene) (p-PPV). Though a series of the single crystals of its derivatives have been demonstrated with high photoluminescence efficiency, their OFETs are still mostly dominated by holes transport.[19, 20] Besides, the influences of the structure and supramolecular interaction to the optoelectronic characters are not very clear. The strong electrophilic cyano group can reduce the lowest unoccupied molecular orbital (LUMO) level without too much change to the highest occupied molecular orbital (HOMO) level which can remarkably improve the electron injection. Meanwhile, it can form strong intramolecular hydrogen bonds which can significantly alter the conformation and molecular packing in the crystal.[21] Considering that, we report the new high-performance ambipolar OFETs prepared from a strong green fluorescent single crystal of cyano-substituted oligo(p-phenylene vinylene) with symmetric electrodes. In the OFETs

based on symmetric calcium electrodes, the electrons can easily by injected into the single-crystal owing to suitable energy match. Moreover, the balanced electron and hole mobilities were demonstrated when the gold was chosen as the source/drain electrodes. And the accumulation threshold voltage is low enough for the OFETs to operate in ambipolar model with the source/drain voltage (V_{ds}) around 50 V despite the high injection barrier. After careful analysing the crystal structure, the high mobility comes from the strong π-π interaction, in addition, the highly order hydrogen bonding matrix (N•••H—C) may create an efficient route to pump the charge to the inner layer which can improve the injection ability.

Experimental section

Crystal growth

The 1,4-bis(2-cyano-2-phenylethenyl)benzene (CNDSB) crystal was grown by the physical vapor transport (PVT) method with a temperature-controlled quartz tube from the synthesized powder. Ultrapure argon was used as the carrier and protection gas to prevent the CNDSB from oxidation at high temperature.[22, 23] A series of growth conditions have been employed to obtain high quality crystals, shown in Table S1. After several hours, some slice-like green crystals and few blue crystals were found hanging inside the wall of the growth tube. All the grown crystals were stored in the ambience.

OFETs fabrication

The p-silicon with 200 nm natural thermal growth SiO_2 was cleaned by acetone and ethanol twice, then immersed in the H_2O_2 and concentrated sulphuric acid (3:7) mixed solution and cleaned by deionized water. The substrate was spin coated with 20 mg/mL Chlorobenzene solution of PMMA at the rate of 2000 rad/min. Then the substrate was annealed on a hotstage at 453 K for 90 s to remove the solvent in the film. The atomic force microscopy (AFM) test shows (performed on SPA300) the roughness of the PMMA film surface is 1.34 nm, and the step profiler (Vecco DEKTAK 150) test shows the thickness of the film is about 70 nm.

The green crystal was transferred to the silicon substrate and pasted to the substrate due to the electrostatic interaction under atmosphere. Then the 300 nm calcium or 250 nm Au electrode was deposited onto the crystal with the rate 0.6 nm/s, 0.3 nm/s under the vacuum below 1.5×10^{-4} Pa.

Electrical characterization

The electrical characterization was performed inside a glovebox by means of semi-conductor parameter analyzer (Agilent Technologies B1500A). Width and length of the channel were measured by a laser scanning confocal microscope (Olympus FV1000), the thickness of the crystal was detected by the step profiler and the XRD of the slice-like crystal was tested by the Rigaku SmartLab with the medium resolution PB model.

Result and Disscussion

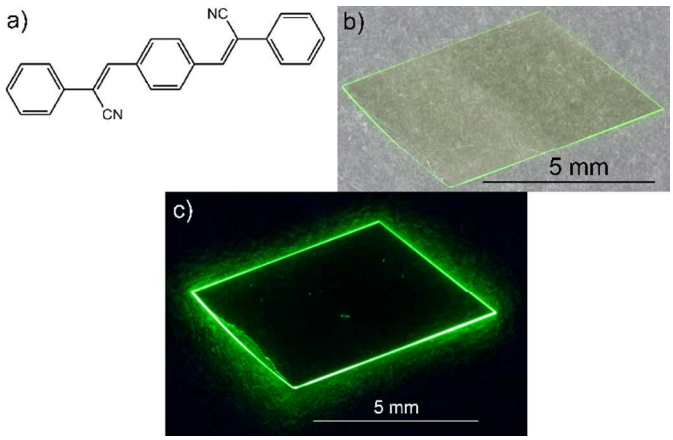

Figure 1. (a) Chemical structure of CNDSB. (b) CNDSB crystal under natural light, the crystal was placed on the vegetable parchment. (c) Fluorescence image of the green crystal.

The chemical structure and fluorescence image of CNDSB crystal grown by the PVT method are shown in Figure 1. The angular slice-like crystals of CNDSB with dozens of microns width and hundreds of microns length are obtained. The transparent crystals show colour of light green under natural light and strong green fluorescence under UV-light. The photoluminescence yield (η_{pl}) reaches up to 75%.[24] The self-waveguided emission was found from the side edges (Figure 1b), which is a premise feature for our further planning for the laser application. The single-crystal OFETs employing the top contact/bottom gate (TC/BG) configuration were fabricated, and the polymethylmethacrylate (PMMA) buffer layer beneficial for the charge transportation was spin-coated on the thermally grown SiO_2.[25] The channel width is 110 μm and the length is 60 μm. In order to evaluate the electron mobility, the calcium was chosen as the source/drain electrodes firstly as considering the energy match between the work function of calcium and LUMO level of CNDSB (figure 3b). The calcium was rapidly de-posited on the CNDSB single crystal to avoid bringing electron traps at the crystal/metal interfaces by trace amounts of oxygen. The FET tests were conducted in the glovebox to protect the calcium electrodes and effectively prevent the formation of electron traps. The observed output and transfer characters were shown in Figure 2a-d. Owing to the LUMO level (-3.26 eV) are slightly lower than the calcium's work function (-2.87 eV), the electrons can easily be injected into the crystal. The accumulation threshold voltage of the OFETs was demonstrated around 20 V, which is much lower than other ambipolar single-crystal OFETs. Typical ohmic contact characters can be observed only at low V_{ds} and low gate voltage (V_g), then disappear at high Vg, suggesting there remains some contact problems in the inter-face, shown in Fig. 2c. On the other hand, it should be noticed that the hole current also was observed in the transfer characteristic though the holes would face a big injection barrier due to the energy mismatch between calcium's work function and the HOMO level of CNDSB single crystal (-6.01 eV). From the P-channel's output curves, one can easily figure out the

accumulate threshold voltage is only around -30 V, that is very interesting when considering energy mismatch is as high as 3.14 eV. Despite the low threshold voltage, there is a large injection barrier for holes which explains the noise output characteristic. In these OFETs, the calculated result shows the mobility of the electron is 0.132 $cm^2V^{-1}s^{-1}$. The hole mobility can't be obtained very accurately owing to the poor injection ability.

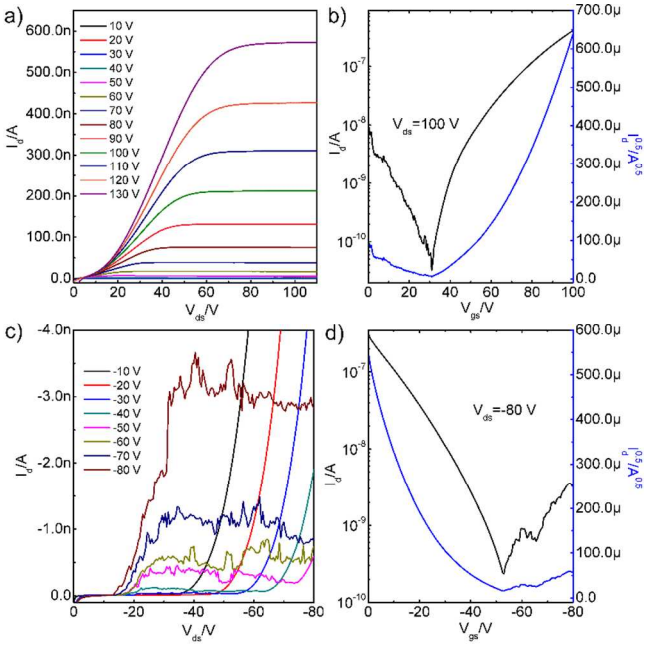

Figure 2. Electrical properties of the OFETs based on symmetric calcium source/drain electrodes, channel width: 110 µm, channel length: 60 µm. (a) Out-put characteristics of N-channel, (c) and P-channel. (b) Transfer character of N-channel, black line: (drain current)1/2, blue line: drain current. (d) Transfer character of P-channel, black line: |drain current|1/2, blue line: lg |drain current|.

Considering the gold's work function is much closer to the CNDSB's HOMO level, the OFETs with the same architecture based on the symmetric gold source/drain electrodes were fabricated. The channel width varies between 10 and 310 µm and the length is 50 to 60 µm. The output and transfer characteristics of the OFETs are shown in Figure 3c-f. The accumulation threshold voltage for electrons and holes are around 30 V and -20 V, respectively. The OFETs can operate in ambipolar model with the V_{ds} only around 50 V (Figure S4a). It's worth noting that the injection barrier for electrons is as high as 1.84 eV (Figure 3b). That is too high to inject the electron efficiently according to current models to elucidate the formation of charge-injection barrier at organic/metal interfaces.[12] From the P-channel output characteristics (Figure 3e), typical nonlinear Schottky behavior[13] was observed. Under a certain V_{ds} with fixed gate voltage (Vg) (e.g. $|V_g|$=60 V, $|V_{ds}|$ <86 V), the devices work as unipolar model, then continued by opposite carrier indicating the ambipolar operation. From the transfer characteristics, it can be perceived that the current of the electrons and holes are very close, and the calculation results show very balanced mobility. With the V_d increasing, the recombination zone is moving to the drain electrode during the gate voltage (V_g) sweeping (Figure S4). In the symmetric FETs, the highest mobility is 0.745 $cm^2V^{-1}s^{-1}$ and 0.239 $cm^2V^{-1}s^{-1}$, and the average mobility is 0.177 $cm^2V^{-1}s^{-1}$ and 0.0457 $cm^2V^{-1}s^{-1}$ for the electron and hole among the 18 devices, respectively. All devices exhibit $I_{on/off}$ ratio higher than 10^5 for both electron and hole at small V_{ds}, while the ratio decreased to less than 10^4 when the V_{ds} is as large as the highest V_{gs} applied during the measurement. The maximum drain current observed for electron and hole is 689 nA and 208 nA, respectively, when

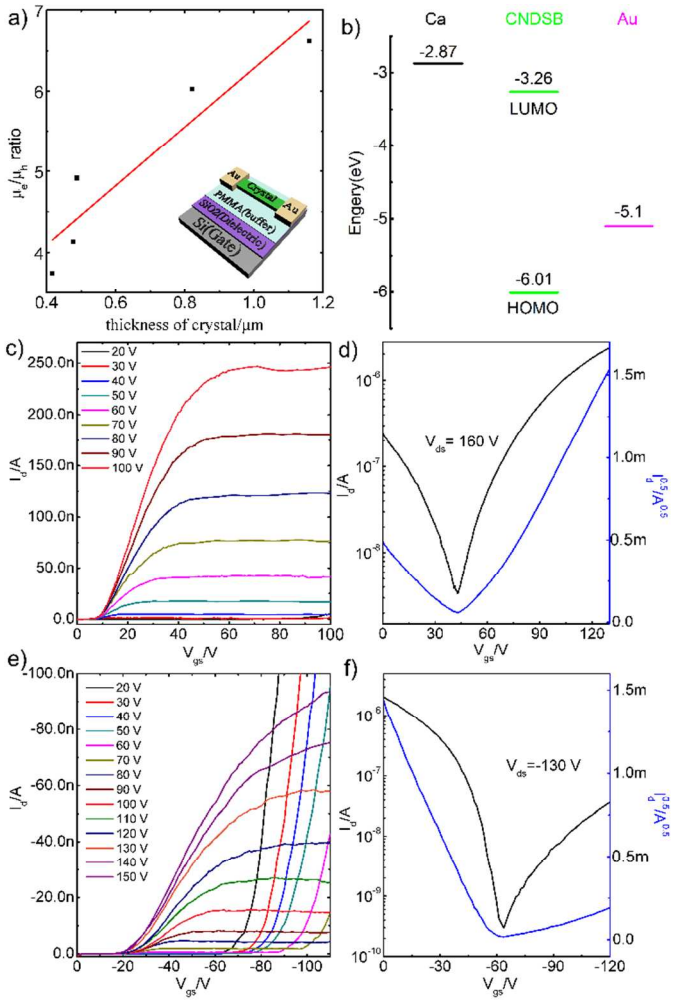

Figure 3. Electrical properties of the OFETs based on symmetric gold source/drain electrodes, channel width: 60 µm, channel length: 60 µm. (a) µe/µh ratio of the OFETs as a function of the crystal thickness, black spot: test result, red line: linear fitting curve. Insert: schematic repre-sentation of the CNDSB single-crystal device. (b) Energy level diagram of CNDSB, comparing with Au and Ca's work function. (c) Out-put characteristics of N-channel, (e) and P-channel. (d) Transfer character of N-channel, black line: (drain current)1/2, blue line: lg (drain current). (f) Transfer character of P-channel, black line: |drain current|1/2, blue line: lg |drain current|.

$|V_g|$=110 V in a device with a channel width of 76 µm (Figure S6), indicating the current density reaches 90.7 A/cm^2 for electron and 27.4 A/cm^2 for hole if we assume the charge accumulation layer thickness was 10 nm.[26] The performance is more balanced than that of most of the reported single-crystal ambipolar OFETs, such as BP3T OFETs, whose hole current

density is 41.2 A/cm^2 in the hole enhancement model, whereas the electron current density is less than 0.04 A/cm^2 in its electron enhancement model even though the calcium/gold asymmetric electrodes were used.[15] Besides, we found that the charge injection depends on the thickness of the crystal. We test the thickness of the CNDSB crystal in each device, as shown in Figure 3a. All the crystals were chosen from the same batch to eliminate the influence of the crystal growth. As the thickness of the crystal increases from 0.4 μm to 1.2 μm, the ratio of the electron to hole mobility increases in almost linear mode.

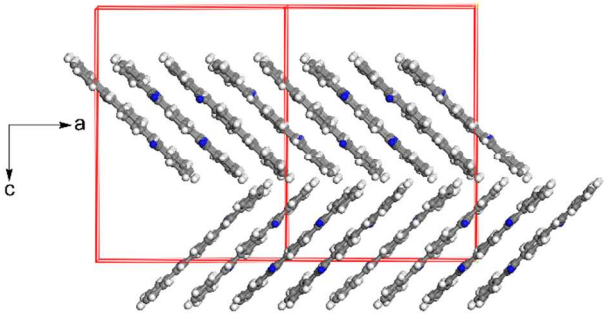

Figure 4. Crystal structures of CNDSB crystal projections on ac-plane.

To reveal the mechanic insight of such high-performance OFET device, X-ray diffraction (XRD) of the CNDSB crystal was conducted, which shows an orthogonal lattice with the space group of Pna21 and cell parameters of a = 19.5 Å, b = 6.929 Å, c = 26.031 Å, Z = 4, respectively. The molecules stack into molecule columns through π-π interaction along a-axis one atop another with a certain displacement along the long molecule axis (Figure 4), and the distance between the adjoining π-plane is 3.394 Å. Such intermolecular arrangement is a typical J-type aggregation, which corresponds to the very high PL efficiency. The multiple hydrogen bonds interconnect the adjacent molecule columns with each other along the b-axis to form layer-like molecule packing. Furthermore, the layer-by-layer structure with herringbone stacking be-tween adjacent layers formed as shown in Figure 4. To define the facets of the slice-like crystal, the parallel light XRD tests were performed. The pattern with the slice-like crystal lying on the substrate is shown in Figure S2a. According to the pattern, the diffraction spacing is 13.096 Å, which matches the thickness of one layers along the c-axis. Some weak (202) (203) and (403) diffraction signals were also detected in the test. Furthermore, the XRD pattern with the crystal standing up was performed, as shown in Figure S2b. Though the diffraction peaks were very weak since the crystal was too thin to achieve efficient diffractions, the signal of (200) (201) and (202) facets can still be distinguished. Besides, the crystals exhibit strong interaction and often fracture neatly along the longest axis. The XRD analysis determined that the top face, long and short side facets were assigned to (001), (010) and (100) planes, respectively (Figure S3). The results indicate the carrier migrating along the channel created by π-π interaction during devices operating, which may correspond to the high mobility of CNDSB crystal.

In the case of trans-DSB, the PVT grown single-crystal is demonstrated an orthorhombic lattice with four molecule in the unit cell. The molecules stack with each other along the long axis, forming the typical H-aggregation.[27, 28] In the lattice, the trans-DSB shows herringbone arrangement with tremendous offset of the adjoining π-planes which can't form strong intermolecular electron coupling. As the cyano groups are introduced, the CN-DSB molecules are stretched as a straight line along the b-axis by the strong N•••H—C hydrogen bonding, resulting in the molecular stacking in the unit cell changing to the typical J-type aggregation and forming strong π-π interactions which is important for high mobility. Comparing with trans-2,5-diphenyl-1,4-distyrylbenzene crystal, another derivative of trans-DSB, the molecular backbone changes to a twisted conformation8 due to the strong repulsion force between the introduced two phenyl groups and the core of the CNDSB. As a result, the distance between the adjoining π-plane is expanded to 3.574 Å. And the twisted conformation also reduces the degree of conjugation. Therefore, the mobility of electron and hole were demonstrated only 0.013 cm^{2}V^{-1}s^{-1} and 0.055 cm^{2}V^{-1}s^{-1}, one order lower than those in CNDSB crystals. The mobility and crystal information of trans-DSB, CNDPDSB and CNDSB are listed in Table S2.

According to the XRD analysis, a large number of cyano-groups are exposed to the side edge of the crystal. The cyano is a very strong coordination group with gold atom[29], thus as gold deposited on the surface of CNDSB crystal, the strong coordination interaction between the cyano and gold can reduce the distance of gold with organic surface which may increase the probability of electron tunnelling at the gold/crystal interface. On the other hand, owing to the cyano group's strong electrophilic characters, the ordered N•••H—C hydrogen bonding network may create an efficient route to pump the injected electron to the inner layer and depopulate the charge density in the interface, which can avoid too much electron accumulating at the metal-crystal interface and enhance the electron injection.

Conclusions

In conclusion, the hydrogen bonds change the common packing model (herringbone arrangement) in the single-crystal of the OPV derivatives to the face to face π-π stacking with a certain displacement. The strong π-π interaction provides strong intermolecular electron coupling, which is beneficial for high carrier mobility. The strong Au-CN interaction in the interface and the N•••H—C hydrogen bonding network may promote the charge injection during the devices operating. Typical ambipolar characters were observed from the ambipolar single-crystal OFETs based on the high fluorescent CNDSB single-crystal with single comment source/drain electrodes, especially when the symmetric gold electrodes was employed. The devices exhibit outstanding and balanced mobility. The CNDSB is very promising for the LE-OFETs and an excellent model material for the fundamental research in the organic electronics.

Acknowledgements

This work was supported by National Science Foundation of China (NFSC) (Grant No. 51103054, 91233113) and Ministry of Science and Technology of China (Grant No. 2013CB834705).

Notes and references

[a] State Key Laboratory of Supramolecular Structure and Materials,
[b] College of Chemistry, Jilin University, 2699 Qianjin Avenue, Changchun, 130012,
[c] State Key Laboratory of Luminescent Materials and Devices, South China University of Technology, Guangzhou, 510640, P. R. China

1. J. Huang, X. Yang, X. J. Li, P. Y. Chen, R. L. Tang, F. Li, P. Lu, Y. G. Ma, L. Wang, J. G. Qin, Q. Q. Li and Z. Li, *Chem. Commun.*, 2012, 48, 9586-9588.
2. Freek J. M. Hoeben, Pascal Jonkheijm, E. W. Meijer and A. P. H. J. Schenning, *Chem. Rev.*, 2005, 105, 1491-1546.
3. G. P. Bartholomew, X. H. Bu and G. C. Bazan, *Chem. Mater.*, 2000, 12, 2311-2318.
4. Huibiao Liu , Jialiang Xu , Yongjun Li and Y. Li, *Acc. Chem. Res.*, 2010, 43, 1496-1508.
5. Y. Li, T. Liu, H. Liu, M. Z. Tian and Y. Li, *Acc. Chem. Res.*, 2014, 47, 1186-1198.
6. C. Reese and Z. Bao, *J. Mater. Chem.*, 2006, 16, 329.
7. Z. Xie, B. Yang, F. Li, G. Cheng, L. Liu, G. Yang, H. Xu, L. Ye, M. Hanif, S. Liu, D. Ma and Y. Ma, *J. Am. Chem. Soc.*, 2005, 127, 14152-14153.
8. H. Wang, F. Li, B. R. Gao, Z. Q. Xie, S. J. Liu, C. L. Wang, D. H. Hu, F. Z. Shen, Y. X. Xu, H. Shang, Q. D. Chen, Y. G. Ma and H. B. Sun, *Cryst. Growth Des.*, 2009, 9, 4945-4950.
9. T. Yamao, K. Yamamoto, Y. Taniguchi, T. Miki and S. Hotta, *J. Appl. Phys.*, 2008, 103, 093115.
10. T. Hasegawa and J. Takeya, *Sci. Technol. Adv. Mat.*, 2009, 10, 024314.
11. R. J. Tseng, R. Chan, V. C. Tung and Y. Yang, *Adv. Mater.*, 2008, 20, 435-438.
12. C. Fan, A. P. Zoombelt, H. Jiang, W. Fu, J. Wu, W. Yuan, Y. Wang, H. Li, H. Chen and Z. Bao, *Adv. Mater.*, 2013, 25, 5762-5766.
13. H. Nakanotani, M. Saito, H. Nakamura and C. Adachi, *Appl. Phys. Lett.*, 2009, 95, 103307.
14. H. T. Yi, Y. Chen, K. Czelen and V. Podzorov, *Adv. Mater.*, 2011, 23, 5807-5811.
15. S. Z. Bisri, T. Takenobu, Y. Yomogida, H. Shimotani, T. Yamao, S. Hotta and Y. Iwasa, *Adv. Funct. Mater.*, 2009, 19, 1728-1735.
16. T. Takahashi, T. Takenobu, J. Takeya and Y. Iwasa, *Adv. Funct. Mater.*, 2007, 17, 1623-1628.
17. M. Kitamura and Y. Arakawa, *J. Phys.: Condens. Mat.*, 2008, 20, 184011.
18. T. Takahashi, T. Takenobu, J. Takeya and Y. Iwasa, *Appl. Phys. Lett.*, 2006, 88, 033505.
19. H. Nakanotani, R. Kabe, M. Yahiro, T. Takenobu, Y. Iwasa and C. Adachi, *Appl. Phys. Express*, 2008, 1, 091801.
20. H. Nakanotani, M. Saito, H. Nakamura and C. Adachi, *Appl. Phys. Lett.*, 2009, 95.
21. H. Wang, F. Li, I. Ravia, B. Gao, Y. Li, V. Medvedev, H. Sun, N. Tessler and Y. Ma, *Adv. Funct. Mater.*, 2011, 21, 3770-3777.
22. R. A. Laudise, C. Kloc, P. G. Simpkins and T. Siegrist, *J. Cryst. Growth*, 1998, 187, 449-454.
23. H. Wang, F. Li, B. Gao, Z. Xie, S. Liu, C. Wang, D. Hu, F. Shen, Y. Xu, H. Shang, Q. Chen, Y. Ma and H. Sun, *Cryst. Growth Des.*, 2009, 9, 4945-4950.
24. X. J. Li, Y. X. Xu, F. Li and Y. G. Ma, *Org. Electron.*, 2012, 13, 762-766.
25. V. Janos, O. Simon and L. Giles, *Chem. Mater.*, 2004, 16, 4543-4555.
26. H. Wang, J. Wang, H. Huang, X. Yan and D. Yan, *Org. Electron.*, 2006, 7, 369-374.
27. J. Gierschner, L. Lueer, B. Milian-Medina, D. Oelkrug and H.-J. Egelhaaf, *J. Phys. Chem. Lett.*, 2013, 4, 2686-2697.
28. C. C. Wu, M. C. DeLong, Z. V. Vardeny and J. P. Ferraris, *Synth. Met.*, 2003, 137, 939-941.
29. B. Cui, H.-J. Yan, D. Wang and L.-J. Wan, *J. Electroanal. Chem.*, 2013, 688, 237-242.

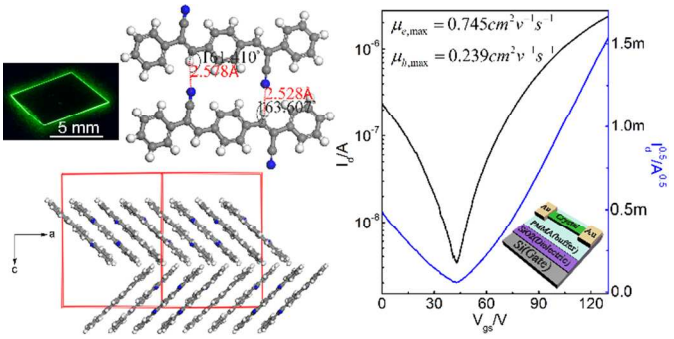

High performance symmetric OFETs made by strong green florescent single-crystals were demonstrated well-balanced mobilities of around 0.5 $cm^2V^{-1}s^{-1}$.